MASTER'S DEGREE THESIS

Master of Science in Advanced Mathematics and Mathematical Engineering

Title: Numerical modelling of the growth of glioblastoma cells in microfluidic devices

Author: Maria Elzaurdi Carrera

Advisor: Dr. José Sarrate Ramos

Department: Departament d'Enginyeria Civil i Ambiental (751)

Academic year: 2021-2022

UNIVERSITAT POLITÈCNICA DE CATALUNYA
BARCELONATECH
Facultat de Matemàtiques i Estadística

Universitat Politècnica de Catalunya
Facultat de Matemàtiques i Estadística

Master in Advanced Mathematics and Mathematical Engineering

Master's thesis

Numerical modelling of the growth of glioblastoma cells in microfluidic devices

Maria Elzaurdi

Supervised by José Sarrate Ramos

June, 2022

I would like to express my gratitude to my supervisor José Sarrate Ramos for his academic and personal help, for his time, his patience and above all, for believing in me. It has been a pleasure to meet him and an honour to learn from him.

To my parents, my two sisters and Asier for supporting me throughout this academic year, thanks to their love and support the journey has been much easier.

Finally, I would also like to thank my friends from the Basque Country and Barcelona who have always been by my side.

Abstract

Glioblastoma Multiform (GBM) tumour is considered one of the most aggressive and lethal primary brain tumour. *In vivo* trials are complex due to the amount of different variables that can affect a human body, collateral damages and ethical issues. To overcome these problems, *in vitro* experiments are done using a microfluidic device. However, these experiments are still expensive in terms of time and human resources. Thus, numerical models are needed in order to design these devices and reduce the total cost of the corresponding experiment.
This project provides an in-depth analysis of a non-linear diffusion-convection-reaction mathematical model considering the interaction of the tumour cells with oxygen concentration. The numerical resolution of this model is done by using high-order continuous finite elements method and high-order Diagonally Implicit Runge-Kutta, DIRK, temporal discretization schemes. Hence, we end up with a non-linear system at each time stage which is solved applying the Newton-Raphson's method. Finally, we present several examples that illustrate the capabilities of the presented formulation.

Keywords

Glioblastoma Multiform, numerical modelling, finite element method, non-linear equations, Newton Raphson, oxygen, living cells, dead cells.

Contents

List of Figures

1. Introduction

Glioblastoma Multiform, GBM, is an aggressive type of cancer that appears in the brain as well as in the spinal cord. In most of the cases it can be difficult to cure, and there are a few treatments that slow its growth and alleviate its symptoms.

In a human body, cells are in contact with the micro-environment and they receive external stimuli all time. This make them modify their shape, their location, they tend to migrate, and so on [7, 8]. *In vivo* research of this situation is difficult and dangerous due to the consequences that these experiments can have on the quality life of the patients. In order to acquire a deeper knowledge on the evolution of this type of tumour, *in vitro* experiments are used, so that we have a better control of the variables [1]. These experiments have been done in 2D where cells are mostly cultured in the traditional Petri dish, in which cell behaviour is very different from the observed in real cases [2, 9]. To overcome these drawbacks, microfluidic devices were designed to allow a more accurate reproduction of the micro-environment and cell distributions [1], including three-dimensionality.

Figure 1 presents a 2D sketch of a generic microfluidic device. It is composed of a central micro-chamber where GBM cells are seeded at a prescribed density in a collagen hydrogel. This chamber is surrounded by two microchannels that are used to supply oxygen to GBM cells through several holes that can be opened or closed depending on the ongoing experiment.

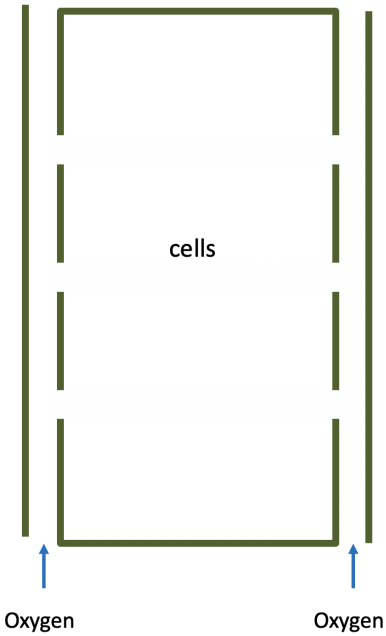

Figure 1: 2D sketch of a microfluidic device.

The main cell processes considered are cell proliferation, differentiation and migration in total relation with oxygen concentration surrounding the cell. In addition, two types of experiments will be simulated with these microfluidic devices. First, oxygen will be supplied from both microchannels when high concentration of living cells is inserted in the microchamber. Living cells quickly consume the existing oxygen and start to dye and migrate towards both microchannels. This way, a necrotic core is generated at the inner part of the

microchamber. Second, oxygen will be supplied from one single microchannel when a lower concentration of living cells is inserted in the microchannel. In this case, cells migrate towards the open microchannel more slowly than in the necrotic core case and a pallisade of living cells is generated at the open channel. These two type of experiments will be illustrated in figures 2 and 3 obtained from reference [1].

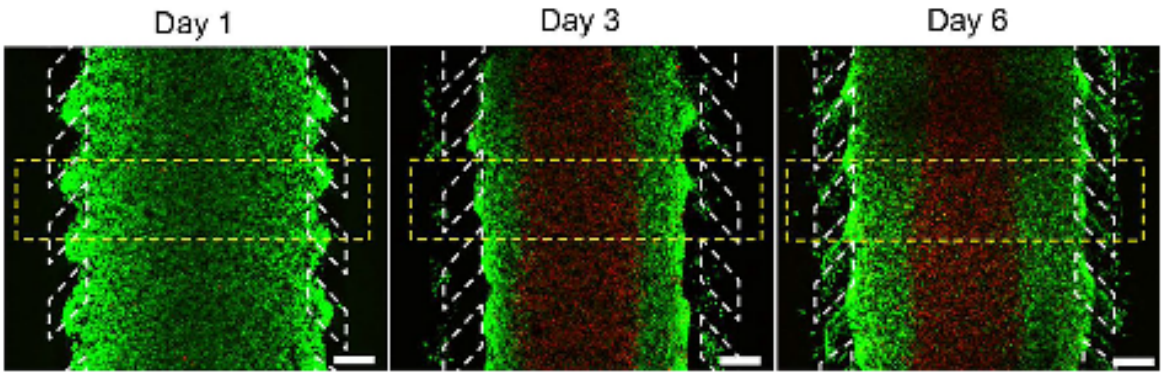

Figure 2: Three snapshots of an experiment where a necrotic core is generated.

Dead cells are marked in red and living cells are marked in green. After oxygen is depleted, living cells "dye" or move towards lateral walls so a necrotic core is created to the inner part of the micro chamber (figure from reference [1]).

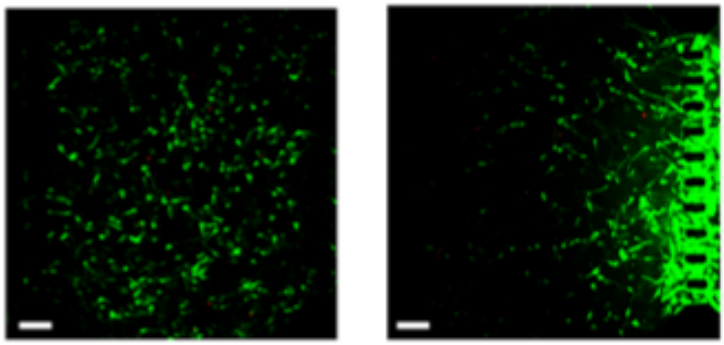

Figure 3: Two snapshots of an experiment where a single pallisade is generated.

The left image shows initial living cells distribution while the right one presents living cells distribution once oxygen is supplied by the right channel, forming a single pallisade (figure from reference [1]).

These trials take a long time to complete them and if the design of the devices is complex even more time is needed. After a long number of experiments, it has been observed that the dimension of the device and its geometry have a strong influence on the duration of the experiment. In order to reduce the time and to make the process more manageable, the versatility of mathematical modelling and computational methods are used to analyse the growth of glioblastoma cancer [5, 6].

Glioblastoma Multiform tumour is the most common and aggressive of the primary gliomas. Therefore, special efforts are focused on the development of new drugs and therapies that can lead to a better prognosis. To this end, in this work, a mathematical model for the growth of the glioblastoma cells in microfluidic devices is developed. It is based on a system of non-linear partial differential equations and

ordinary differential equations. In order to compute the numerical solution for this non-linear diffusion-convection-reaction model, high order finite element and implicit DIRK time discretization methods are used.

This master thesis is structured in six chapters. Chapter 1, briefly introduces the main characteristics of the physical problem and sets the objectives of this work. In chapter 2 the mathematical model used throughout the work is presented. Chapter 3 details how we solve the problem by means of spatial and temporal discretization methods. In the fourth chapter, some implementation details are discussed. Chapter 5 presents several examples in 2D and 3D. Finally, in chapter 6, we explain the conclusions of this work and analyse the future work.

2. Mathematical Model

2.1 General Formulation

The general formulation of the Glioblastoma Multiform growth evolution is provided by the next mathematical model composed by a non-linear diffusion-convection-reaction equations. Tumour cell growth is modelled using a non-linear coupled system:

$$\frac{\partial c^i}{\partial t} + \boldsymbol{\nabla} \cdot \mathbf{f}^i = s^i \qquad \text{for } i = 0, 1, \dots, n. \tag{1}$$

where c^0 is the oxygen concentration and c^i for $i = 1, \dots, n$ are the concentrations of the n phenotypes of cells. $\mathbf{f}^i$ is the corresponding flux and s^i represents the source term of each element. The motion of these phenotypes are governed by a diffusion term (proportional to the gradient of each concentration) and a chemotaxis part (proportional to the gradient of oxygen concentration):

$$\mathbf{f}^i = -\mathbf{A}^i \boldsymbol{\nabla} c^i + c^i \mathbf{B}^i \boldsymbol{\nabla} c^0 \qquad \text{for } i = 0, \dots, n.$$

where $\mathbf{A}^i$ and $\mathbf{B}^i$ are the diffusion and chemotaxis matrices. In general, these coefficients depend on temperature, mechanical cues (represented by $\mathbf{E}$) and the concentration of the oxygen and the phenotypes ($\mathbf{c} = (c^0, c^1, \dots, c^n)^T$). Hence, they can be expressed as $\mathbf{A}^i = \mathbf{A}^i(\mathbf{E}, T, \mathbf{c})$ and $\mathbf{B}^i = \mathbf{B}^i(\mathbf{E}, T, \mathbf{c})$. The source terms are modelled as:

$$\begin{aligned} s^0 &= -\sum_{j=1}^{n} \alpha^j c^j \\ s^i &= \frac{1}{\tau_{ii}} c^i - \sum_{j=1, j\neq i}^{n} \frac{1}{\tau_{ij}} c^i + \sum_{j=1, j\neq i}^{n} \frac{1}{\tau_{ji}} c^j \qquad i = 1, \dots, n. \end{aligned}$$

where $\alpha^i = \alpha^i(\mathbf{E}, T, c^0)$ is is the oxygen rate consumed by the i-th cell population depending on the temperature, mechanical cues and oxygen concentration, $\tau_{ii} = \tau_{ii}(\mathbf{E}, T, \mathbf{c})$ is the characteristic time of proliferation for population i and $\tau_{ij} = \tau_{ij}(\mathbf{E}, T, \mathbf{c})$ corresponds to the characteristic time of differentiation form population i to j, both of them depending also on the temperature, mechanical cues and concentrations. Specifically, for application in microfluidic devices where living cells are mixed with hydrogel at constant temperature, the thermal and mechanical dependences can be neglected.

This system is completed with a set of some initial and boundary conditions.

$$\begin{cases} c^i(x,t) = g_D^i & \text{for } \; x \in \Gamma_D^i \\ \mathbf{f}^i \cdot \mathbf{n} = g_N^i & \text{for } \; x \in \Gamma_N^i \\ \mathbf{f}^i \cdot \mathbf{n} = \beta^i (c^i - g_R^i) & \text{for } \; x \in \Gamma_R^i \\ c^i(x,0) = c^{i,0}(x) & \forall x \in \Omega \end{cases}$$

where Ω is the domain and its contour is $\partial\Omega = \Gamma_D^i \cup \Gamma_N^i \cup \Gamma_R^i$ for $i = 0, ..., n$.

2.2 Particular case

In this work we are considering two phenotypes cells: living cells concentration, c^1, and dead cells concentration, c^2. Similarly, we denote by c^0 to the continuum field of oxygen concentration. Thus, we shall denote by $\mathbf{c} = (c^0, c^1, c^2)^T$ the vector of field variables with 3 rows. Then, the equation that regulates each population evolution can be expressed by considering different assumptions based on [2]:

1. **Oxygen**: The general case for oxygen concentration is:

$$\frac{\partial c^0}{\partial t} + \boldsymbol{\nabla} \cdot \mathbf{f}^0 = s^0$$

$$\mathbf{f}^0 = -\mathbf{A}^0 \boldsymbol{\nabla} c^0$$

   The assumptions make in the oxygen case are (see reference [2] for more details):

   (a) $\mathbf{A^0}$ is constant.

   (b) $\mathbf{B^0} = 0$, this means that oxygen does not move respect to its gradient.

   (c) The oxygen consumed per unit time by the living cells is

$$\alpha^1 = \alpha^1_* r(c^0; c^0_t) c^1$$

   where α^1_* is a constant, c^0_t is the oxygen concentration related to the oxidative phosphorylation kinetics, the cell structure and morphology and the diffusion process in the cytoplasm and $r(c^0; c^0_t)$ is a function of the oxygen concentration which describes more accurately the consumption at low oxygen concentration:

$$r(c^0; c^0_t) = \frac{c^0}{c^0 + c^0_t}$$

   As dead cells do not consume oxygen it is considered that $\alpha_2 = 0$. Thus, the source term for the oxygen equation becomes

$$s^0 = -\alpha^1_* \, r(c^0; c^0_t) \, c^1 \tag{2}$$

2. **Living cells**: The general case for living cells concentration is:

$$\frac{\partial c^1}{\partial t} + \boldsymbol{\nabla} \cdot \mathbf{f}^1 = s^1$$

$$\mathbf{f}^1 = -\mathbf{A}^1 \boldsymbol{\nabla} c^1 + c^1 \mathbf{B}^1 \boldsymbol{\nabla} c^0$$

   The following assumptions are considered (see reference [2] for more details):

   (a) $\mathbf{A^1}$ is constant.

   (b) $\mathbf{B^1}$ is related to the oxygen and living cells concentration:

$$\mathbf{B^1} = B^1_* \beta^1(c^0, c^1)$$

   where B^1_* is a constant value and β^1 regulates how chemotaxis and proliferation/differentiation are activated depending on oxygen and cell population concentrations. This last term is defined as

$$\beta^1(c^0, c^1) = \phi_-(c^0; c^0_h)\phi_-(c^1; c^1_s)$$

where c_s^1 is the cell saturation concentration and c_h^0 the induced hypoxia migration activation threshold. The functions are defined as ReLU functions:

$$\phi_{\text{-}}(c^1; c_s^1) = \begin{cases} 1 & \text{if } c^1 < 0 \\ 1 - \frac{c^1}{c_s^1} & \text{if } 0 \leq c^1 \leq c_s^1 \\ 0 & \text{if } c^1 > c_s^1 \end{cases}$$

$$\phi_{\text{-}}(c^0; c_h^0) = \begin{cases} 1 & \text{if } c^0 < 0 \\ 1 - \frac{c^0}{c_h^0} & \text{if } 0 \leq c^0 \leq c_h^0 \\ 0 & \text{if } c^0 > c_h^0 \end{cases}$$

(c) It is considered that dead cells cannot be converted into living cells, this means that $\tau_{21}^{-1} = 0$. Then, the source term is modelled as

$$s^1 = \tau_{11}^{-1} c^1 + \tau_{12}^{-1} c^1 = \frac{1}{\tau_{11}^*} S_{11}(c^0, c^1) c^1 + \frac{1}{\tau_{12}^*} S_{12}(c^0) c^1$$

where τ_{11}^* and τ_{12}^* are a constant values, τ_{11} is the characteristic time of proliferation for living cells and τ_{12} is the characteristic time of differentiation from living cells to dead cells. In our case,

$$S_{11}(c^0, c^1) = \phi_+(c^0; c_h^0) \rho(c^1; c_s^1)$$

Besides that, cell proliferation also depends on nutrient supply or availability of space to grow and split. Thus, the model combines logistic growth and the go or grow paradigm based on oxygen supply. We define the growth corrections as:

$$\begin{aligned} \phi_+(c^0; c_h^0) &= \begin{cases} 0 & \text{if } c^0 < 0 \\ \frac{c^0}{c_h^0} & \text{if } 0 \leq c^0 \leq c_h^0 \\ 1 & \text{if } c^0 > c_h^0 \end{cases} \\ \rho(c^1; c_s^1) &= (1 - \frac{c^1}{c_s^1}) \end{aligned}$$

Moreover,

$$S_{12}(c^0) = \frac{1}{2}(1 - \tanh(\frac{c^0 - c_a^0}{\Delta c_a^0}))$$

where c_a^0 and Δc_a^0 are the location and the spread parameters associated to the oxygen concentration inducing cell death.

3. **Dead cells**: The general case for dead cells concentration is:

$$\frac{\partial c^2}{\partial t} + \boldsymbol{\nabla} \cdot \mathbf{f}^2 = s^2$$

$$\mathbf{f}^2 = 0$$

Dead cells are considered as an inert population. Based on experimental observation [2], we assume

(a) $\mathbf{A^2} = 0$.

(b) $\mathbf{B^2} = 0$.

(c) We consider that dead cells are just created from living cells. Then, $\tau_{21}^{-1} = \tau_{22}^{-1} = 0$, while

$$\frac{1}{\tau_{12}} = \frac{1}{\tau_{12}^*} S_{12}(c^0)$$

where τ_{12}^* is a constant and $S_{12}(c^0)$ is a function that depends on c^0. Thus, the source term is

$$s^2 = \frac{1}{\tau_{12}^*} S_{12}(c^0)\, c^1 .$$

Once the equations for our model are posed, the values of the parameters that we have already explained must be defined. Many of them are essentially unknown or with high ranges of variation. In order to determine a set of reliable values for these parameters, in references [1] and [2] a parametric analysis based on a 1D models have been developed. Table 1 details the values proposed in these works and the ones that will be used here. It is important to point out that all of them are in the range found in bibliography:

name	**value**	**units**
O_2 diffusion (A^0)	10^{-5}	cm^2/s
O_2 consumption rate (α_*^1)	10^{-9}	mmHg $\times$ cm^3
Michaelis-Menten constant (c_t^0)	2.5	mmHg
cell diffusion (A^1)	6.6×10^{-10}	cm^2/s
chemotaxis coefficient (B_*^1)	7.5×10^{-9}	cm^2 / (mmHg $\times$ s)
hipoxia migration threshold (c_h^0)	7	mmHg
cell saturation limit (c_s^1)	5×10^7	cell/mL
growth characteristic time (τ_{11}^*)	7.2×10^5	s
deadth characteristic time (τ_{12}^*)	1.728×10^5	s
anoxia death threshold (c_a^0)	1.6	mmHg
anoxia death sensibility (Δc_a^0)	0.1	mmHg

Table 1: The parameters values

.

3. Numerical Model

Once the previously explained assumptions are applied, the model to solve is:

$$\frac{\partial c^0}{\partial t} - \boldsymbol{\nabla} \cdot (\mathbf{A}^0 \boldsymbol{\nabla} c^0) = s^0 \tag{3}$$

$$\frac{\partial c^1}{\partial t} + \boldsymbol{\nabla} \cdot (-\mathbf{A}^1 \boldsymbol{\nabla} c^1 + c^1 \mathbf{B}^1 \boldsymbol{\nabla} c^0) = s^1 \tag{4}$$

$$\frac{\partial c^2}{\partial t} = s^2 \tag{5}$$

This non-linear diffusion-convection-reaction mathematical model can be solved by applying numerical methods that involve high-order continuous Finite Element method and high order Diagonally Implicit Runge-Kutta (DIRK) time schemes. This leads to a non-linear problem at each stage of the DIRK scheme that will be solved by the Newton method.

3.1 Weak form

We consider the space of test functions

$$V_0^i = \{v \in H^1(\Omega) \,:\, v_{|\Gamma_D^i} = 0\} \qquad \text{for } i = 0, 1, 2$$

where Γ_D^i denotes the Dirichlet boundary for the i-th species, and the set of admissible functions

$$V_D^i = \{v \in H^1(\Omega) \,:\, v_{|\Gamma_D^i} = g^i\} \qquad \text{for } i = 0, 1.$$

The non-linear equations for oxygen and living cells contain the divergence of the flux. Therefore, they can be solved in a similar manner. Considering the equations for both of them as:

$$\frac{\partial c^i}{\partial t} + \boldsymbol{\nabla} \cdot \mathbf{f}^i = s^i \qquad \text{for } i = 0, 1. \tag{6}$$

Multiplying both sides by a test function, $\psi^i \in V_0^i$ for $i = 0, 1$ we have

$$\int_\Omega \psi^i \frac{\partial c^i}{\partial t} \mathrm{d}\Omega + \int_\Omega \psi^i \boldsymbol{\nabla} \cdot \mathbf{f}^i \mathrm{d}\Omega = \int_\Omega \psi^i s^i \mathrm{d}\Omega \qquad \text{for } i = 0, 1.$$

Applying integration by parts and the divergence theorem in the flux term, we obtain for all $\psi^i \in V_0^i$,

$$\int_\Omega \psi^i \frac{\partial c^i}{\partial t} d\Omega + \int_{\partial\Omega} \psi^i \mathbf{f}^i \cdot \mathbf{n} d\Gamma - \int_\Omega \nabla \psi^i \cdot \mathbf{f}^i d\Omega = \int_\Omega \psi^i s^i d\Omega \quad \text{for } i = 0, 1$$

Considering now the boundary conditions that we have described before and substituting the flux value, we obtain for $i = 0, 1$:

$$\int_\Omega \psi^i \frac{\partial c^i}{\partial t} d\Omega + \int_\Omega \boldsymbol{\nabla} \psi^i \cdot \mathbf{A}^i \boldsymbol{\nabla} c^i d\Omega - \int_\Omega \boldsymbol{\nabla} \psi^i \cdot (c^i \mathbf{B}^i \boldsymbol{\nabla} c^0) d\Omega + \int_{\Gamma_R^i} \psi^i \beta^i c^i d\Gamma$$

$$= \int_\Omega \psi^i s^i d\Omega - \int_{\Gamma_N^i} \psi^i g_N^i d\Gamma + \int_{\Gamma_R^i} \psi^i \beta^i g_R^i d\Gamma$$

The case of dead cells is the easiest due to the fact that flux is not considered. The equation to solve is:

$$\frac{\partial c^2}{\partial t} = s^2$$

where $c^2(x,t) \in H^1(\Omega)$. Multiplying each part by a test function $\psi^2 \in H^1(\Omega)$ and integrating in the corresponding domain, we obtain

$$\int_\Omega \psi^2 \frac{\partial c^2}{\partial t} d\Omega = \int_\Omega \psi^2 s^2 d\Omega$$

Then, the weak formulation of our problem reads: find $(c^0, c^1) \in (V_D^0, V_D^1)$ such that

$$\begin{aligned} &\int_\Omega \psi^i \frac{\partial c^i}{\partial t} \mathrm{d}\Omega + \int_\Omega \boldsymbol{\nabla}\psi^i \cdot \mathbf{A}^i \boldsymbol{\nabla} c^i \mathrm{d}\Omega - \int_\Omega \boldsymbol{\nabla}\psi^i \cdot (c^i \mathbf{B}^i \boldsymbol{\nabla} c^0) \mathrm{d}\Omega + \int_{\Gamma_R^i} \psi^i \, \beta^i \, c^i \, \mathrm{d}\Gamma \\ &= \int_\Omega \psi^i s^i \mathrm{d}\Omega - \int_{\Gamma_N^i} \psi^i h^i \mathrm{d}\Gamma + \int_{\Gamma_R^i} \psi^i \beta^i g_N^i \, \mathrm{d}\Gamma \qquad \text{for } i = 0, 1. \end{aligned} \tag{7}$$

for all $(\psi^0, \psi^1) \in (V_0^0, V_0^1)$ and find $c^2 \in V_0^2$

$$\int_\Omega \psi^2 \frac{\partial c^2}{\partial t} d\Omega = \int_\Omega \psi^2 s^2 d\Omega$$

for all $\psi^2 \in V_0^2$.

3.2 Spatial discretization

First of all, we discretize in space our unknown $c^i(x,t) \in V_D^i$ which is defined as

$$c^i(x,t) = \sum_{j=1}^{n_u^i} N_j(x) c_j^i(t) + \sum_{k=n_u^i+1}^{n_t} N_k(x) c_k^i(t)$$

where n_t represents the total number of nodes and n_u the number of nodes in which the concentration c^i is unknown. Then, we are going to divide our concentrations in two summations: on the one hand, we have the sum of the unknown concentrations while on the other hand, the known concentrations are summed. Replacing the approximation in the weak form, we obtain: find $c_j^i(t) \in \mathbb{R}$ for any $t > 0$ and for $i = 0, 1$ such that

$$\begin{aligned} &\sum_{j=1}^{n_u^i} \frac{dc_j^i}{dt} \int_\Omega N_l N_j d\Omega + \sum_{j=1}^{n_u^i} c_j^i \int_\Omega \boldsymbol{\nabla} N_l \cdot \mathbf{A^i} \boldsymbol{\nabla} N_j d\Omega \\ &- \sum_{j=1}^{n_u^i} c_j^i \int_\Omega \boldsymbol{\nabla} N_l \cdot (N_j \mathbf{B^i} (\sum_{r=1}^{n_t} c_r^0 \boldsymbol{\nabla} N_r) d\Omega + \sum_{j=1}^{n_u^i} c_j^i \int_{\Gamma_R^i} \alpha^i N_l N_j d\Gamma \\ &= \int_\Omega N_l s^i d\Omega - \int_{\Gamma_N^i} N_l h^i d\Gamma + \int_{\Gamma_R^i} N_l \beta^i g_R^i d\Gamma \\ &- \sum_{j=n_u^i+1}^{n_t} \frac{dc_j^i}{dt} \int_\Omega N_l N_j d\Omega - \sum_{j=n_u^i+1}^{n_t} c_j^i \int_\Omega \boldsymbol{\nabla} N_l \cdot \mathbf{A^i} \boldsymbol{\nabla} N_j d\Omega \\ &+ \sum_{j=n_u^i+1}^{n_t} c_j^i \int_\Omega \boldsymbol{\nabla} N_l \cdot (N_j \mathbf{B^i} (\sum_{r=1}^{n_t} c_r^0 \boldsymbol{\nabla} N_r) d\Omega + \sum_{j=n_u^i+1}^{n_t} c_j^i \int_{\Gamma_R^i} \beta^i N_l N_j d\Gamma \end{aligned} \tag{8}$$

for all $l = 1, ..., n_u^i$.
With regard to dead cells, our unknown $c^2(x,t) \in H^1(\Omega)$ is discretized by

$$c^2(x,t) = \sum_{j=1}^{n_t} N_j(x) c_j^2(t)$$

Hence, replacing it in the weak form and taking $\psi = N_l$ the expression obtained is: find $c_j^2(t) \in \mathbb{R}$ for any $t > 0$ such that

$$\sum_{j=1}^{n_t} \frac{\partial c_j^2}{\partial t} \int_\Omega N_l N_j d\Omega = \int_\Omega N_l s^2 d\Omega \tag{9}$$

for $l = 1, ..., n_t$. Note that here, we are assuming that no dead cells move outside of the microchannels and only no flux conditions will be applied on all boundaries.

3.3 Temporal discretization

Once spatial discretization is done, we have to carry out the temporal discretization. For this purpose, different techniques can be used. In this work, DIRK schemes are used (more details in [3] and [4]).
Equations (8) and (9) can be discretized in time using DIRK schemes. We use the following notation: $(\cdot)^n$ indicates the value of any variable at time t^n and $(\cdot)^{n,l}$ the value of any variable at time $t^{n,l} = t^n + c_l \Delta t$, where n denotes the time step and l the DIRK stage. Hence, the concentration of any component at time $t^{n+1} = t^n + \Delta t$ will be:

$$c^{i,n+1} = c^{i,n} + \Delta t \sum_{l=1}^{s} b_l \dot{c}^{i,n,l}, \tag{10}$$

where $\dot{c}^{i,n,l}$ is the approximation of dc^i/dt at time $t^{n,l}$, and s is the total number of stages. The solution at each stage of the DIRK scheme is computed as:

$$c^{i,n,l} = c^{i,n} + \Delta t \sum_{k=1}^{l} a_{lk} \dot{c}^{i,n,k}$$

Considering $\hat{c}^{i,n,l} = c^{i,n} + \Delta t \sum_{k=1}^{l-1} a_{lk} \dot{c}^{i,n,k}$, the solution at each stage can be computed as:

$$c^{i,n,l} = \hat{c}^{i,n,l} + \Delta t a_{ll} \dot{c}^{i,n,l} \qquad \text{for } l = 1, \dots, s, \tag{11}$$

By clearing the derivative parameter from the previous equation we obtain

$$\dot{c}^{i,n,l} = \frac{c^{i,n,l} - \hat{c}^{i,n,l}}{\Delta t \, a_{ll}} \qquad \text{for } l = 1, \dots, s, \tag{12}$$

Parameters b_l, c_l, a_{lk} define the DIRK method and are given by the Butcher's table, see Table 2. Note that for DIRK schemes matrix **A** is lower triangular, as it is considered in equation (11).

Table 2: Butcher's table for a diagonal implicit Runge-Kutta scheme.

$$\begin{array}{c|c} \mathbf{c} & \mathbf{A} \\ \hline & \mathbf{b} \end{array} \equiv \begin{array}{c|cccc} c_1 & a_{11} & & & \\ c_2 & a_{21} & a_{22} & & \\ \vdots & \vdots & & \ddots & \\ c_s & a_{s1} & & \dots & a_{ss} \\ \hline & b_1 & b_2 & \dots & b_s \end{array}$$

In the oxygen and living cells cases, at stage l of the step n, that is, at $t^{n,l}$ and for $i = 0, 1$, we look for $c_\beta^{i,n,l} \in \mathbb{R}$ so that

$$\begin{aligned}
&\sum_{\beta=1}^{n_u^i} \dot{c}_\beta^{i,n,l} \int_\Omega N_\alpha N_\beta \mathrm{d}\Omega + \sum_{\beta=1}^{n_u^i} c_\beta^{i,n,l} \int_\Omega \boldsymbol{\nabla} N_\alpha \cdot \mathbf{A}^i \boldsymbol{\nabla} N_\beta \mathrm{d}\Omega \\
&- \sum_{\beta=1}^{n_u^i} c_\beta^{i,n,l} \int_\Omega \boldsymbol{\nabla} N_\alpha \cdot \Big(N_\beta \mathbf{B}^{i,n,l} \Big(\sum_{r=1}^{n_n} c_r^{0,n,l} \boldsymbol{\nabla} N_r \Big) \Big) \mathrm{d}\Omega + \sum_{\beta=1}^{n_u^i} c_\beta^{i,n,l} \int_{\Gamma_R^i} \beta^{i,n,l} N_\alpha N_\beta \mathrm{d}\Gamma \\
&= \int_\Omega N_\alpha s^{i,n,l} \mathrm{d}\Omega - \int_{\Gamma_N^i} N_\alpha h^{i,n,l} \mathrm{d}\Gamma - \int_{\Gamma_R^i} N_\alpha \alpha^{i,n,l} g_R^{i,n,l} \mathrm{d}\Gamma \\
&- \sum_{\beta=n_u^i+1}^{n_t} \dot{c}_\beta^{i,n,l} \int_\Omega N_\alpha N_\beta \mathrm{d}\Omega - \sum_{\beta=n_u^i+1}^{n_t} c_\beta^{i,n,l} \int_\Omega \boldsymbol{\nabla} N_\alpha \cdot \mathbf{A}^i \boldsymbol{\nabla} N_\beta \mathrm{d}\Omega \\
&+ \sum_{\beta=n_u^i+1}^{n_t} c_\beta^{i,n,l} \int_\Omega \boldsymbol{\nabla} N_\alpha \cdot \Big(N_\beta \mathbf{B}^{i,n,l} \Big(\sum_{r=1}^{n_t} c_r^{0,n,l} \boldsymbol{\nabla} N_r \Big) \Big) \mathrm{d}\Omega \\
&+ \sum_{\beta=n_u^i+1}^{n_t} c_\beta^{i,n,l} \int_{\Gamma_R^i} \beta^{i,n,l} N_\alpha N_\beta \mathrm{d}\Gamma
\end{aligned} \tag{13}$$

for $\alpha = 1, \dots, n_u^i$.

Introducing equation (12) into equation (13) we obtain that at time $t^{n,l}$ and for $i = 0, 1$, we seek for $c_\beta^{i,n,l} \in \mathbb{R}$ such that

$$
\begin{aligned}
&\sum_{\beta=1}^{n_u^i} c_\beta^{i,n,l} \int_\Omega N_\alpha N_\beta \mathrm{d}\Omega + a_{ll}\,\Delta t \sum_{\beta=1}^{n_u^i} c_\beta^{i,n,l} \int_\Omega \boldsymbol{\nabla} N_\alpha \cdot \mathbf{A}^i \boldsymbol{\nabla} N_\beta \mathrm{d}\Omega \\
&- a_{ll}\,\Delta t \sum_{\beta=1}^{n_u^i} c_\beta^{i,n,l} \int_\Omega \boldsymbol{\nabla} N_\alpha \cdot \Big(N_\beta \mathbf{B}^{i,n,l} \Big(\sum_{r=1}^{n_t} c_r^{0,n,l} \boldsymbol{\nabla} N_r \Big) \Big) \mathrm{d}\Omega \\
&+ a_{ll}\,\Delta t \sum_{\beta=1}^{n_u^i} c_\beta^{i,n,l} \int_{\Gamma_R^i} \beta^{i,n,l} N_\alpha N_\beta \,\mathrm{d}\Gamma \\
&= a_{ll}\,\Delta t \int_\Omega N_\alpha s^{i,n,l} \mathrm{d}\Omega + \sum_{\beta=1}^{n_u^i} \hat{c}_\beta^{i,n,l} \int_\Omega N_\alpha N_\beta \mathrm{d}\Omega \\
&- a_{ll}\,\Delta t \int_{\Gamma_N^i} N_\alpha h^{i,n,l} \mathrm{d}\Gamma + a_{ll}\,\Delta t \int_{\Gamma_R^i} N_\alpha \beta^{i,n,l} g_R^{i,n,l} \,\mathrm{d}\Gamma \\
&- \sum_{\beta=n_u^i+1}^{n_t} \big(c_\beta^{i,n,l} - \hat{c}_\beta^i \big) \int_\Omega N_\alpha N_\beta \mathrm{d}\Omega - a_{ll}\,\Delta t \sum_{\beta=n_u^i+1}^{n_t} c_\beta^{i,n,l} \int_\Omega \boldsymbol{\nabla} N_\alpha \cdot \mathbf{A}^i \boldsymbol{\nabla} N_\beta \mathrm{d}\Omega \\
&+ a_{ll}\,\Delta t \sum_{\beta=n_u^i+1}^{n_t} c_\beta^{i,n,l} \int_\Omega \boldsymbol{\nabla} N_\alpha \cdot \Big(N_\beta \mathbf{B}^{i,n,l} \Big(\sum_{r=1}^{n_t} c_r^{0,n,l} \boldsymbol{\nabla} N_r \Big) \Big) \mathrm{d}\Omega \\
&+ a_{ll}\,\Delta t \sum_{\beta=n_u^i+1}^{n_t} c_\beta^{i,n,l} \int_{\Gamma_R^i} \beta^{i,n,l} N_\alpha N_\beta \,\mathrm{d}\Gamma
\end{aligned}
\tag{14}
$$

for $\alpha = 1, \dots, n_u^i$.

In the case of dead cells, at time $t^{n,l}$, we seek for $c_\beta^{2,n,l} \in \mathbb{R}$ such that

$$
\sum_{\beta=1}^{n_t} \dot{c}_\beta^{2,n,l} \int_\Omega N_\alpha N_\beta \mathrm{d}\Omega = \int_\Omega N_\alpha s^{2,n,l} \mathrm{d}\Omega \tag{15}
$$

for $\alpha = 1, \dots, n_n$.

Inserting equation (12) into equation (15), we obtain that at time $t^{n,l}$ we seek for $c_\beta^{2,n,l} \in \mathbb{R}$ such that

$$
\sum_{\beta=1}^{n_t} c_\beta^{2,n,l} \int_\Omega N_\alpha N_\beta \mathrm{d}\Omega = a_{ll}\,\Delta t \int_\Omega N_\alpha s^{2,n,l} \mathrm{d}\Omega + \sum_{\beta=1}^{n_t} \hat{c}_\beta^{2,n,l} \int_\Omega N_\alpha N_\beta \mathrm{d}\Omega \tag{16}
$$

for $\alpha = 1, \dots, n_n$.

Equation (14) and (16) are a system of non-linear equations that we rewrite using the residual form:

$$
\mathbf{R}\big(\mathbf{c}^{0,n,l}, \mathbf{c}^{1,n,l}, \mathbf{c}^{2,n,l}\big) = \begin{pmatrix} \mathbf{R}^0\big(\mathbf{c}^{0,n,l}, \mathbf{c}^{1,n,l}, \mathbf{c}^{2,n,l}\big) \\ \mathbf{R}^1\big(\mathbf{c}^{0,n,l}, \mathbf{c}^{1,n,l}, \mathbf{c}^{2,n,l}\big) \\ \mathbf{R}^2\big(\mathbf{c}^{0,n,l}, \mathbf{c}^{1,n,l}, \mathbf{c}^{2,n,l}\big) \end{pmatrix} = \begin{pmatrix} \mathbf{0} \\ \mathbf{0} \\ \mathbf{0} \end{pmatrix} . \tag{17}
$$

We now particularize (17) to our case taking into account the hypotheses on the data and coefficients indicated in previous chapter. Next we detail, for $i = 0, 1, 2$, the αth component R_α^i of the vector $\mathbf{R}^i$.

1. The residual form for the oxygen case is:

$$
\begin{aligned}
R_\alpha^0 \;=\; & \sum_{\beta=1}^{n_u^0} c_\beta^{0,n,l} \int_\Omega N_\alpha N_\beta \mathrm{d}\Omega + a_{II}\,\Delta t \sum_{\beta=1}^{n_u^0} c_\beta^{0,n,l} \int_\Omega \boldsymbol{\nabla} N_\alpha \cdot \mathbf{A}^0 \boldsymbol{\nabla} N_\beta \mathrm{d}\Omega \\
& + a_{II}\,\Delta t \sum_{\beta=1}^{n_u^0} c_\beta^{0,n,l} \int_{\Gamma_R^0} \beta^{0,n,l} N_\alpha N_\beta \,\mathrm{d}\Gamma \\
& - a_{II}\,\Delta t \int_\Omega (-1)\alpha_*^1 N_\alpha \, r(\mathbf{c}^{0,n,l}; c_t^0) \Big(\sum_{r=1}^{n_t} c_r^{1,n,l} N_r \Big) \mathrm{d}\Omega - \sum_{\beta=1}^{n_u^0} \hat{c}_\beta^{0,n,l} \int_\Omega N_\alpha N_\beta \mathrm{d}\Omega \qquad (18) \\
& + a_{II}\,\Delta t \int_{\Gamma_N^0} N_\alpha h^{0,n,l} \mathrm{d}\Gamma - a_{II}\,\Delta t \int_{\Gamma_R^0} N_\alpha \beta^{0,n,l} g_R^{0,n,l} \,\mathrm{d}\Gamma \\
& + \sum_{\beta=n_u^i+1}^{n_t} \left(c_\beta^{0,n,l} - \hat{c}_\beta^0 \right) \int_\Omega N_\alpha N_\beta \mathrm{d}\Omega + a_{II}\,\Delta t \sum_{\beta=n_u^0+1}^{n_t} c_\beta^{0,n,l} \int_\Omega \boldsymbol{\nabla} N_\alpha \cdot \mathbf{A}^0 \boldsymbol{\nabla} N_\beta \mathrm{d}\Omega \\
& - a_{II}\,\Delta t \sum_{\beta=n_u^0+1}^{n_t} c_\beta^{0,n,l} \int_{\Gamma_R^0} \beta^{0,n,l} N_\alpha N_\beta \,\mathrm{d}\Gamma
\end{aligned}
$$

for $\alpha = 1, \dots, n_u^0$.

2. The residual form for the living cells is:

$$
\begin{aligned}
R^1_\alpha \;=\; & \sum_{\beta=1}^{n^1_u} c^{1,n,l}_\beta \int_\Omega N_\alpha N_\beta \mathrm{d}\Omega + a_{II}\,\Delta t \sum_{\beta=1}^{n^1_u} c^{1,n,l}_\beta \int_\Omega \boldsymbol{\nabla} N_\alpha \cdot \mathbf{A}^1 \boldsymbol{\nabla} N_\beta \mathrm{d}\Omega \\
& - a_{II}\,\Delta t \sum_{\beta=1}^{n^i_u} c^{1,n,l}_\beta \int_\Omega \boldsymbol{\nabla} N_\alpha \cdot \Big(N_\beta \mathbf{B}^{1,n,l} \Big(\sum_{r=1}^{n_t} c^{0,n,l}_r \boldsymbol{\nabla} N_r \Big) \Big) \mathrm{d}\Omega \\
& + a_{II}\,\Delta t \sum_{\beta=1}^{n^1_u} c^{1,n,l}_\beta \int_{\Gamma^1_R} \beta^{1,n,l} N_\alpha N_\beta \,\mathrm{d}\Gamma \\
& - a_{II}\,\Delta t \int_\Omega N_\alpha \left(\frac{1}{\tau^*_{11}} S_{11}(\mathbf{c}^{0,n,l}, \mathbf{c}^{1,n,l}) - \frac{1}{\tau^*_{12}} S_{12}(\mathbf{c}^{0,n,l}) \right) \Big(\sum_{r=1}^{n_t} c^{1,n,l}_r N_r \Big) \mathrm{d}\Omega \\
& - \sum_{\beta=1}^{n^0_u} \hat{c}^{1,n,l}_\beta \int_\Omega N_\alpha N_\beta \mathrm{d}\Omega \\
& + a_{II}\,\Delta t \int_{\Gamma^1_N} N_\alpha h^{1,n,l} \mathrm{d}\Gamma - a_{II}\,\Delta t \int_{\Gamma^1_R} N_\alpha \beta^{1,n,l} g^{1,n,l}_R \,\mathrm{d}\Gamma \\
& + \sum_{\beta=n^i_u+1}^{n_t} \left(c^{1,n,l}_\beta - \hat{c}^1_\beta \right) \int_\Omega N_\alpha N_\beta \mathrm{d}\Omega + a_{II}\,\Delta t \sum_{\beta=n^1_u+1}^{n_t} c^{1,n,l}_\beta \int_\Omega \boldsymbol{\nabla} N_\alpha \cdot \mathbf{A}^1 \boldsymbol{\nabla} N_\beta \mathrm{d}\Omega \\
& - a_{II}\,\Delta t \sum_{\beta=n^1_u+1}^{n_t} c^{1,n,l}_\beta \int_\Omega \boldsymbol{\nabla} N_\alpha \cdot \Big(N_\beta \mathbf{B}^{1,n,l} \Big(\sum_{r=1}^{n_t} c^{0,n,l}_r \boldsymbol{\nabla} N_r \Big) \Big) \mathrm{d}\Omega \\
& - a_{II}\,\Delta t \sum_{\beta=n^1_u+1}^{n_t} c^{1,n,l}_\beta \int_{\Gamma^1_R} \beta^{1,n,l} N_\alpha N_\beta \,\mathrm{d}\Gamma
\end{aligned}
\tag{19}
$$

for $\alpha = 1, \dots, n^1_u$.

3. The residual form for dead cells is:

$$
\begin{aligned}
R^2_\alpha \;=\; & \sum_{\beta=1}^{n_t} c^{2,n,l}_\beta \int_\Omega N_\alpha N_\beta \mathrm{d}\Omega - \frac{a_{II}\,\Delta t}{\tau^*_{12}} \int_\Omega N_\alpha S_{12}(\mathbf{c}^{0,n,l}) \Big(\sum_{r=1}^{n_t} c^{1,n,l}_r N_r \Big) \mathrm{d}\Omega \\
& - \sum_{\beta=1}^{n_t} \hat{c}^{2,n,l}_\beta \int_\Omega N_\alpha N_\beta \mathrm{d}\Omega
\end{aligned}
\tag{20}
$$

for $\alpha = 1, \dots, n^2_u$.

Newton-Raphson method will be used in order to find the roots of (18), (19) and (20). This method consists on solving the linear system for each iteration ν,

$$
\mathbf{J}(\mathbf{c}^{n,l}_\nu)\; \Delta \mathbf{c}_{\nu+1} = -\mathbf{R}(\mathbf{c}^{n,l}_\nu)
$$

where $\Delta \mathbf{c}_{\nu+1} = \mathbf{c}^{n,l}_{\nu+1} - \mathbf{c}^{n,l}_\nu$ and $\mathbf{J}(\mathbf{c}^{n,l}_\nu)$ is the 3×3 block Jacobian matrix with the block in the ith row and jth column defined as

$$
\Big[\mathbf{J}(\mathbf{c}^{n,l}_\nu) \Big]_{ij} = \frac{\partial \mathbf{R}^i}{\partial \mathbf{c}^{j,n,l}_\nu} \qquad i,j = 0,1,2.
$$

This block is a $n_u^i \times n_u^j$ matrix $(i, j = 0, 1, 2)$ whose entries are

$$\left[\frac{\partial \mathbf{R}^i}{\partial \mathbf{c}_\nu^{j,n,l}}\right]_{\alpha\beta} = \frac{\partial R_\alpha^i}{\partial c_{\beta,\nu}^{j,n,l}} \qquad \alpha = 1, \dots, n_u^i,\ \beta = 1, \dots, n_u^j.$$

More precisely, this matrix is computed for each cell concentration:

1. For the oxygen case:

$$\begin{aligned}
\left[\frac{\partial \mathbf{R}^0}{\partial \mathbf{c}_\nu^{0,n,l}}\right]_{\alpha\beta} &= \frac{\partial R_\alpha^0}{\partial c_{\beta,\nu}^{0,n,l}} \\
&= \int_\Omega N_\alpha N_\beta \mathrm{d}\Omega + a_{ll}\,\Delta t \int_\Omega \boldsymbol{\nabla} N_\alpha \cdot \mathbf{A}^0 \boldsymbol{\nabla} N_\beta \mathrm{d}\Omega + a_{ll}\,\Delta t \int_{\Gamma_R^0} \beta^{0,n,l} N_\alpha N_\beta \mathrm{d}\Gamma \\
&\quad - a_{ll}\,\Delta t \int_\Omega (-1)\alpha_*^1 N_\alpha \frac{\partial r(\mathbf{c}_\nu^{0,n,l}; c_t^0)}{\partial c^0} N_\beta \Big(\sum_{r=1}^{n_t} c_{r,\nu}^{1,n,l} N_r \Big) \mathrm{d}\Omega \qquad (21) \\
&\quad \text{for } \alpha, \beta = 1, \dots, n_u^0\,; \\
\left[\frac{\partial \mathbf{R}^0}{\partial \mathbf{c}_\nu^{1,n,l}}\right]_{\alpha\beta} &= \frac{\partial R_\alpha^0}{\partial c_{\beta,\nu}^{1,n,l}} \\
&= - a_{ll}\,\Delta t \int_\Omega (-1)\alpha_*^1 r(\mathbf{c}_\nu^{0,n,l}; c_t^0)\, N_\alpha N_\beta \mathrm{d}\Omega \qquad (22) \\
&\quad \text{for } \alpha = 1, \dots, n_u^0 \text{ and } \beta = 1, \dots n_u^1\,; \\
\left[\frac{\partial \mathbf{R}^0}{\partial \mathbf{c}_\nu^{2,n,l}}\right]_{\alpha\beta} &= \frac{\partial R_\alpha^0}{\partial c_{\beta,\nu}^{2,n,l}} = 0 \qquad (23) \\
&\quad \text{for } \alpha = 1, \dots, n_u^0 \text{ and } \beta = 1, \dots n_t^2\,.
\end{aligned}$$

2. For the living cells:

$$\left[\frac{\partial \mathbf{R}^1}{\partial \mathbf{c}_\nu^{0,n,l}}\right]_{\alpha\beta} = \frac{\partial R_\alpha^1}{\partial c_{\beta,\nu}^{0,n,l}}$$

$$= -a_{ll}\,\Delta t \int_\Omega \boldsymbol{\nabla} N_\alpha \cdot \left(\Big(\sum_{r=1}^{n_t} c_{r,\nu}^{1,n,l} N_r \Big) \left(\left.\frac{\partial \mathbf{B}_n u^1}{\partial c^0}\right|_{\mathbf{c}_\nu^{n,l}} N_\beta \Big(\sum_{r=1}^{n_t} c_{r,\nu}^{0,n,l} \boldsymbol{\nabla} N_r \Big) + \mathbf{B}_\nu^{1,n,l} \boldsymbol{\nabla} N_\beta \right) \right) \mathrm{d}\Omega$$

$$-a_{ll}\,\Delta t \int_\Omega N_\alpha \left(\frac{1}{\tau_{11}^*} \left.\frac{\partial S_{11}}{\partial c^0}\right|_{\mathbf{c}_\nu^{n,l}} - \frac{1}{\tau_{12}^*} \left.\frac{\partial S_{12}}{\partial c^0}\right|_{\mathbf{c}_\nu^{0,n,l}} \right) N_\beta \Big(\sum_{r=1}^{n_t} c_{r,\nu}^{1,n,l} N_r \Big) \mathrm{d}\Omega \tag{24}$$

for $\alpha = 1, \ldots, n_u^1$ and $\beta = 1, \ldots n_u^0$;

$$\left[\frac{\partial \mathbf{R}^1}{\partial \mathbf{c}_\nu^{1,n,l}}\right]_{\alpha\beta} = \frac{\partial R_\alpha^1}{\partial c_{\beta,\nu}^{1,n,l}}$$

$$= \int_\Omega N_\alpha N_\beta \mathrm{d}\Omega + a_{ll}\,\Delta t \int_\Omega \boldsymbol{\nabla} N_\alpha \cdot \mathbf{A}^1 \boldsymbol{\nabla} N_\beta \mathrm{d}\Omega$$

$$-a_{ll}\,\Delta t \int_\Omega \boldsymbol{\nabla} N_\alpha \cdot \left(\Big(B_\nu^{1,n,l} + \Big(\sum_{r=1}^{n_t} c_{r,\nu}^{1,n,l} N_r \Big) \left.\frac{\partial \mathbf{B}^1}{\partial c^1}\right|_{\mathbf{c}_\nu^{n,l}} \Big) N_\beta \Big(\sum_{r=1}^{n_t} c_{r,\nu}^{0,n,l} \boldsymbol{\nabla} N_r \Big) \right) \mathrm{d}\Omega$$

$$+a_{ll}\,\Delta t \int_{\Gamma_R^1} \beta^{1,n,l} N_\alpha N_\beta \,\mathrm{d}\Gamma$$

$$-a_{ll}\,\Delta t \int_\Omega N_\alpha \frac{1}{\tau_{11}^*} \left.\frac{\partial S_{11}}{\partial c^1}\right|_{\mathbf{c}_\nu^{n,l}} N_\beta \Big(\sum_{r=1}^{n_t} c_{r,\nu}^{1,n,l} N_r \Big) \mathrm{d}\Omega$$

$$-a_{ll}\,\Delta t \int_\Omega N_\alpha \left(\frac{1}{\tau_{11}^*} S_{11}(\mathbf{c}_\nu^{0,n,l}, \mathbf{c}_\nu^{1,n,l}) - \frac{1}{\tau_{12}^*} S_{12}(\mathbf{c}_\nu^{0,n,l}) \right) N_\beta \,\mathrm{d}\Omega \tag{25}$$

for $\alpha, \beta = 1, \ldots, n_u^1$;

$$\left[\frac{\partial \mathbf{R}^1}{\partial \mathbf{c}_\nu^{2,n,l}}\right]_{\alpha\beta} = \frac{\partial R_\alpha^1}{\partial c_{\beta,\nu}^{2,n,l}} = 0 \tag{26}$$

for $\alpha = 1, \ldots, n_u^1$ and $\beta = 1, \ldots n_t^2$.

3. For the dead cells:

$$\begin{aligned}
\left[\frac{\partial \mathbf{R}^2}{\partial \mathbf{c}_\nu^{0,n,l}}\right]_{\alpha\beta} &= \frac{\partial R_\alpha^2}{\partial c_{\beta,\nu}^{0,n,l}} \\
&= -\frac{a_{II}\,\Delta t}{\tau_{12}^*}\int_\Omega N_\alpha \left.\frac{\partial S_{12}}{\partial c^0}\right|_{\mathbf{c}_\nu^{0,n,l}} N_\beta\Big(\sum_{r=1}^{n_t} c_{r,\nu}^{1,n,l} N_r\Big)\mathrm{d}\Omega \qquad (27)\\
&\quad \text{for } \alpha = 1,\dots,n_t \text{ and } \beta = 1,\dots n_u^0\,; \\
\left[\frac{\partial \mathbf{R}^2}{\partial \mathbf{c}_\nu^{1,n,l}}\right]_{\alpha\beta} &= \frac{\partial R_\alpha^2}{\partial c_{\beta,\nu}^{1,n,l}} \\
&= -\frac{a_{II}\,\Delta t}{\tau_{12}^*}\int_\Omega N_\alpha S_{12}(\mathbf{c}_\nu^{0,n,l}) N_\beta \mathrm{d}\Omega \qquad (28)\\
&\quad \text{for } \alpha = 1,\dots,n_t \text{ and } \beta = 1,\dots n_u^1\,; \\
\left[\frac{\partial \mathbf{R}^2}{\partial \mathbf{c}_\nu^{2,n,l}}\right]_{\alpha\beta} &= \frac{\partial R_\alpha^2}{\partial c_{\beta,\nu}^{2,n,l}} \\
&= \int_\Omega N_\alpha N_\beta \mathrm{d}\Omega \qquad (29)\\
&\quad \text{for } \alpha,\beta = 1,\dots,n_t^2\,.
\end{aligned}$$

Taking all these computations into account the Jacobian matrix structure is:

$$\mathbf{J} = \begin{bmatrix} \mathbf{J_{00}} & \mathbf{J_{00}} & \mathbf{0} \\ \mathbf{J_{10}} & \mathbf{J_{10}} & \mathbf{0} \\ \mathbf{J_{20}} & \mathbf{J_{20}} & \mathbf{J_{22}} \end{bmatrix}$$

Finally, once the concentrations are known at all stages the corresponding time derivatives at all stages are computed using equation (12). From these values, the concentration at time step $n+1$ is computed according to equation (11).

4. Implementation Details

As detailed in chapter 3, the non-linear system composed by equations (14) and (16) or (17) in compact form, has to be solved at each stage of the DIRK scheme. In this work, we use the Newton's method to solve it. Therefore, at each iteration of the Newton method the linear system has to be solved. In order to speed up the solution process we exploit the structure of the system matrix. Thus, the linear system to be solved is:

$$\begin{bmatrix} \mathbf{J_{00}} & \mathbf{J_{00}} & \mathbf{0} \\ \mathbf{J_{10}} & \mathbf{J_{10}} & \mathbf{0} \\ \mathbf{J_{20}} & \mathbf{J_{20}} & \mathbf{J_{22}} \end{bmatrix} \begin{bmatrix} \Delta\mathbf{c}^0 \\ \Delta\mathbf{c}^1 \\ \Delta\mathbf{c}^2 \end{bmatrix} = \begin{bmatrix} -\mathbf{R}^0 \\ -\mathbf{R}^1 \\ -\mathbf{R}^2 \end{bmatrix}$$

To speed up the experiments, we are not going to solve the whole system directly. This means that, to reduce the memory footprint and the computational time, we split it in two uncoupled and smaller linear systems. First, we solve it for oxygen and living cells, that is, we seek for $\Delta\mathbf{c}^0$ and $\Delta\mathbf{c}^1$ by solving:

$$\begin{bmatrix} \mathbf{J_{00}} & \mathbf{J_{00}} \\ \mathbf{J_{10}} & \mathbf{J_{10}} \end{bmatrix} \begin{bmatrix} \Delta\mathbf{c}^0 \\ \Delta\mathbf{c}^1 \end{bmatrix} = \begin{bmatrix} -\mathbf{R}^0 \\ -\mathbf{R}^1 \end{bmatrix} \tag{30}$$

Afterwards, using the concentration values obtained before, we can compute the case of dead cells, that is, we seek for $\Delta\mathbf{c}^2$:

$$\mathbf{J_{22}}\Delta\mathbf{c}^2 = -\mathbf{R}^2 - \mathbf{J_{20}}\Delta\mathbf{c}^0 - \mathbf{J_{21}}\Delta\mathbf{c}^1 \tag{31}$$

where the values in the right hand side are known.

We compute the matrix structure of the linear system: one for oxygen and living cells, and the other one for dead cells. We loop on time according to the selected DIRK scheme. At each stage of the DIRK scheme we solve the non-linear residual system. That is, we iterate according to the Newton's method. Thus, at each iteration:

1. We compute the residual for oxygen and living cells, (18) and (19).
2. We compute the Jacobian for oxygen and living cells, (21), (22), (24) and (25).
3. We solve the linear system for oxygen and living cells, (30).

This process is done until convergence conditions are achieved. Once we obtain the values for $\Delta\mathbf{c}^0$ and $\Delta\mathbf{c}^1$, the same steps will be done for dead cells:

1. We compute the residual for dead cells, (20).
2. We compute the Jacobian for dead cells, (27), (28), and (29).
3. We solve the linear system for oxygen and living cells, (31).

We iterate until convergence is achieved. Specifically, the process for oxygen and living cells stops when

$$\begin{aligned} \frac{\|c_\nu^{0,n,l} - c_{\nu+1}^{0,n,l}\|_{L_2}}{\|c_{\nu+1}^{0,n,l}\|_{L_2}} &\leq \epsilon_{c_0} \quad \text{and} \quad \|R_\nu^{0,n,l}\|_2 \leq \epsilon_{R_0} \\ \frac{\|c_\nu^{1,n,l} - c_{\nu+1}^{1,n,l}\|_{L_2}}{\|c_{\nu+1}^{1,n,l}\|_{L_2}} &\leq \epsilon_{c_1} \quad \text{and} \quad \|R_\nu^{1,n,l}\|_2 \leq \epsilon_{R_1} \end{aligned}$$

The iteration process for dead cells stops when these two conditions are satisfied:

$$\frac{\|c_\nu^{2,n,l} - c_{\nu+1}^{2,n,l}\|_{L_2}}{\|c_{\nu+1}^{2,n,l}\|_{L_2}} \leq \epsilon_{c_2} \quad \text{and} \quad \|R_\nu^{2,n,l}\|_2 \leq \epsilon_{R_2}$$

5. Examples

In this section we present several examples that illustrate the capabilities of the presented formulation in 2D and 3D. The 2D examples are going to show us a necrotic core state while 3D simulations present a single pallisade situation.

5.1 2D simulation of a microfluidic device under several working conditions

The main objective of this work is to develop a computational model to predict the behaviour of a microfluidic device. In this section we will analyse a specific model of microfluidic devices and we will simulate it under three different working conditions.

Figure 4 shows the 2D CAD model of a microfluidic device. Its height is 1.35 cm and its width measures 0.3 cm. Boundaries coloured in blue represents solid walls made of polystyrene. The green boundary is an exchange surface through which oxygen is supplied. Finally, the brown boundary represents inlet valves. These valves are used in two different ways. On the one hand, they allow injecting a mixture of living cells and collagen hydrogel. On the other hand, they are used to create three different working environments.

First, they can be closed, acting as a solid wall. This will be denoted as case A later. Second, they can be opened, allowing to supply oxygen to the interior of the micro-chamber (they behave as an exchange surface). This will be denoted as case B later. Third, they are opened allowing to supply oxygen but do not allow living cells leaving the micro-chamber, denoted as case C later.

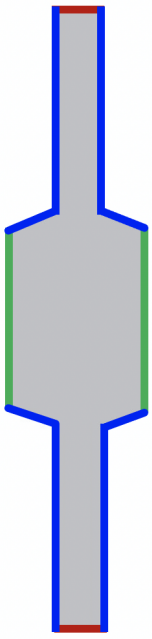

Figure 4: The regions of different boundary conditions in 2D

Next, we summarize the three cases we will analyse and the corresponding boundary conditions at the upper and lower valves.

1. Case A:
   - Oxygen: Neumann homogeneous conditions.
   - Living cells: Neumann homogeneous conditions.
   - Dead cells: Neumann homogeneous conditions.
2. Case B:
   - Oxygen: constant Dirichlet conditions.
   - Living cells: Robin conditions.
   - Dead cells: Neumann homogeneous conditions.
3. Case C:
   - Oxygen: constant Dirichlet conditions.
   - Living cells: Neumann homogeneous conditions.
   - Dead cells: Neumann homogeneous conditions.

The initial conditions in those three cases are the same constant values:

$$\begin{aligned} c^{0,0} &= 7 \text{ mmHg} \\ c^{1,0} &= 4 \times 10^7 \text{ cells/mL} \\ c^{2,0} &= 0 \text{ cell/mL} \end{aligned}$$

For the three cases we have performed two simulations. First, we have used linear elements with Backward Euler time integration scheme. Second, we have used P3 elements with a DIRK3S3 scheme. All simulations have been performed up to a final time step of 3 days and $\Delta t = 1$h.

5.1.1 Case A

As we have already mentioned, what differentiates one case from the other are the boundary conditions at the top and the bottom of the central tube. Specifically, the boundary conditions are:

1. For oxygen:

$$\begin{aligned} \mathbf{f^0} \cdot \mathbf{n} &= 0 \quad \text{in the solid wall.} \\ c^0 &= 7\text{mmHg} \quad \text{in the exchange surface.} \\ \mathbf{f^0} \cdot \mathbf{n} &= 0 \quad \text{in the valves.} \end{aligned}$$

2. For living cells:

$$\begin{aligned} \mathbf{f^1} \cdot \mathbf{n} &= 0 \quad \text{in the solid wall.} \\ \mathbf{f^1} \cdot \mathbf{n} &= \beta^1 c^1 \quad \text{in the exchange surface.} \\ \mathbf{f^1} \cdot \mathbf{n} &= 0 \quad \text{in the valves.} \end{aligned}$$

   with $\beta^1 = 10^{-6}$ s/cm.

3. For dead cells:

$$\begin{aligned} \mathbf{f^2} \cdot \mathbf{n} &= 0 \quad \text{in the solid wall.} \\ \mathbf{f^2} \cdot \mathbf{n} &= 0 \quad \text{in the exchange surface.} \\ \mathbf{f^2} \cdot \mathbf{n} &= 0 \quad \text{in the valves.} \end{aligned}$$

Note that no flux boundary condition is applied on the exchange wall because in the experiments no dead cells have been observed leaving the micro-chamber (see reference [2] for details).

The results of these simulations are presented in figure 5. In the first column, we have used a Backward Euler for the temporal discretization with linear elements while the second one corresponds to DIRK3S3 temporal discretization with elements of degree 3. Red colour expresses the high amount of concentration while blue colour means the opposite, that is, there is a lack of this type of concentration in that part.

At first, we have our mesh full of oxygen and living cells. After 3 days, we can observe that as we imposed Neumann homogeneous conditions everywhere and we supply oxygen concentration in the right and left side, close to these borders is the only place where oxygen remains. With respect to living cells, this type of phenotype just survive near oxygen that is the reason why we only have in red close to these borders. In the remaining part, dead cells appeared due to the lack of oxygen. Hence, the concentration of living cells decreases in the tubes, thus increasing the concentration of dead cells throughout the tube.

Similar results are obtained in both simulations. Table 3 summarizes the characteristics of the used mesh and the computational time of building and solving the linear systems at each stage of the DIRK scheme.

	P1	**P3**
nOfNodes	5763	50311
nOfElements	5504	5504
theNumOfUnknowns of oxygen and live cells	11396	100236
theNumOfUnknowns dead cells	5763	50311
time building the linear system of oxygen and live cells	4.01	5.05
time solving the linear system of oxygen and live cells	0.15	6.12
time building the linear system of dead cells	1.51	1.12
time solving the linear system of dead cells	0.02	0.59
approximated cpu time	1550.22	11875.12

Table 3: Case A, the number of nodes and elements in each problem and the time required to create and solve the system are detailed.

From the images we can state that there is not any significant difference between P1 with Backward Euler and P3 with DIRK3S3. With regard to the table 3, it can be appreciated that working with high-order methods in space and time increase the computational time.

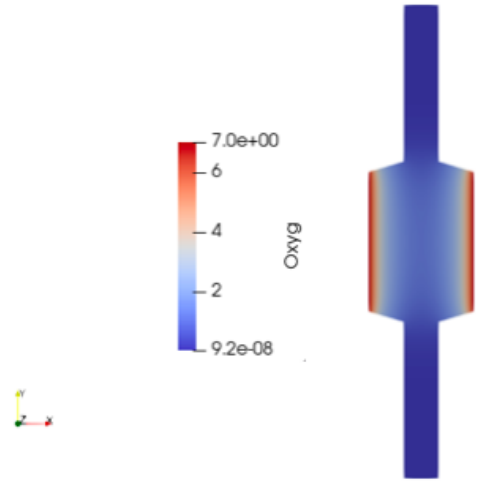

(a) Oxygen case with P1 elements

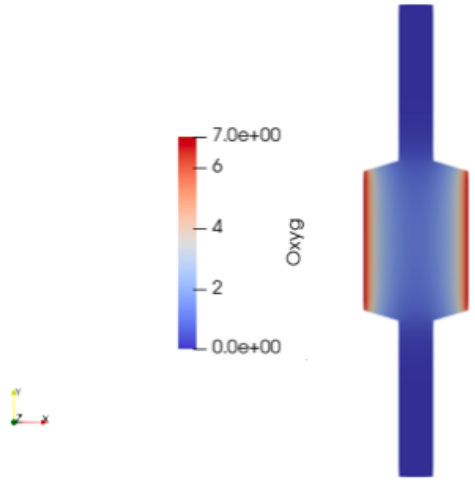

(b) Oxygen case with P3 elements

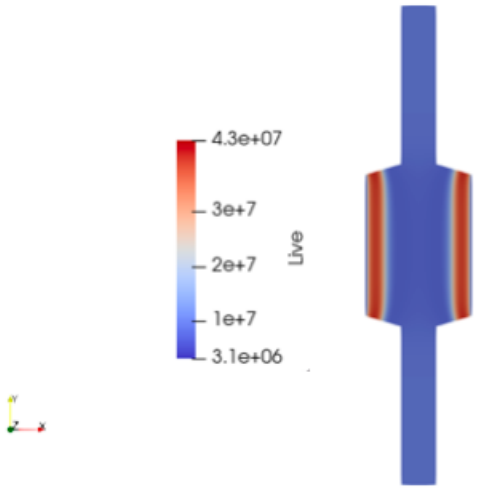

(c) Living cells case with P1 elements

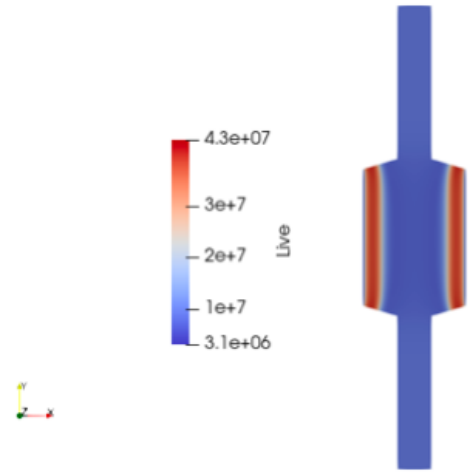

(d) Living cells case with P3 elements

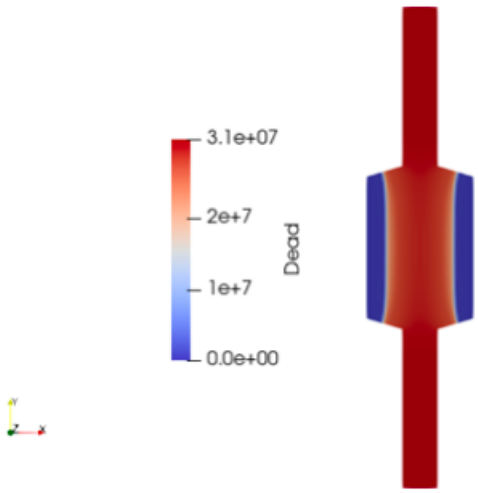

(e) Dead cells case with P1 elements

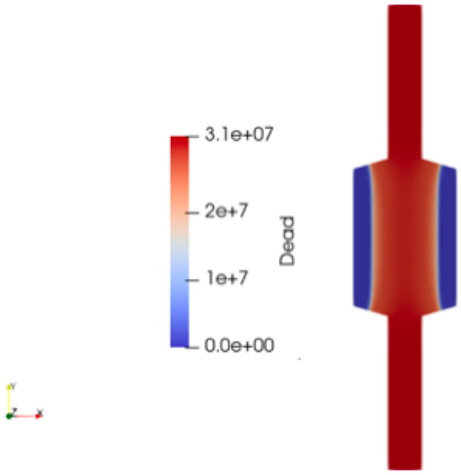

(f) Dead cells case with P3 elements

Figure 5: 2D contour plots for case A of the oxygen, living cells and dead cells after 3 days.

5.1.2 Case B

In this experiment the boundary conditions are different to the previous case. In concrete, the boundary conditions are:

1. For oxygen:

$$\begin{aligned} \mathbf{f^0} \cdot \mathbf{n} &= 0 \quad \text{in the solid wall.} \\ c^0 &= g^0 \quad \text{in the exchange surface.} \\ c^0 &= g^0 \quad \text{in the valves.} \end{aligned}$$

   with $g^0 = 7\text{mmHg}$.

2. For living cells:

$$\begin{aligned} \mathbf{f^1} \cdot \mathbf{n} &= 0 \quad \text{in the solid wall.} \\ \mathbf{f^1} \cdot \mathbf{n} &= \beta^1 c^1 \quad \text{in the exchange surface.} \\ \mathbf{f^1} \cdot \mathbf{n} &= \beta^1 c^1 \quad \text{in the valves.} \end{aligned}$$

   with $\beta^1 = 10^{-6}$ s/cm

3. For dead cells:

$$\begin{aligned} \mathbf{f^2} \cdot \mathbf{n} &= 0 \quad \text{in the solid wall.} \\ \mathbf{f^2} \cdot \mathbf{n} &= 0 \quad \text{in the exchange surface.} \\ \mathbf{f^2} \cdot \mathbf{n} &= 0 \quad \text{in the valves.} \end{aligned}$$

   Note that no flux boundary condition is applied on the exchange wall because in the experiments no dead cells have been observed leaving the micro-chamber (see reference [2] for details).

The computed results are depicted in figure 6. The first column represents the problem solved with linear elements while the second corresponds to elements of degree 3. Red colour expresses the high amount of concentration while blue colour means that there is less amount of concentration of this type.

This particularity can be seen in figure 6. In the exchange surface, the same phenomenon as in Case A happens. With respect to the valves, as Robin conditions are considered in living cells, the concentration of cells increases near these contours, while the concentration of dead cells decreases in the vicinity of these edges. Moreover, in those valves, as there is a high living cells concentration leaving the micro-chamber, their concentration decreases in the Robin contour, thus forming a palisade at some distance from the Robin contour.

Similar results are obtained in both simulations. Table 4 summarizes the characteristics of the mesh and the time required to build and solve the linear systems at each stage of the DIRK scheme.

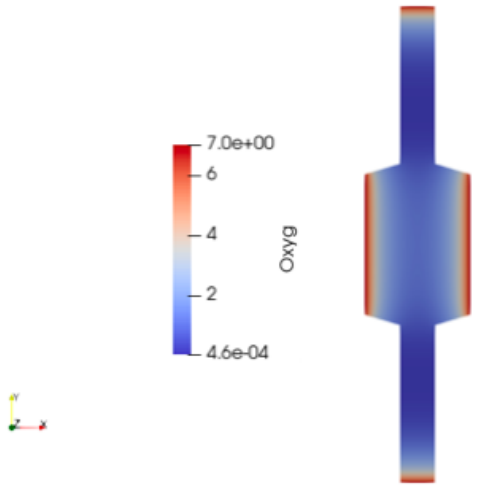

(a) Oxygen case with P1 elements

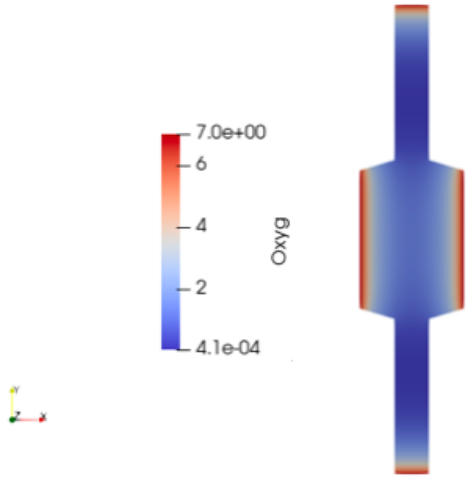

(b) Oxygen case with P3 elements

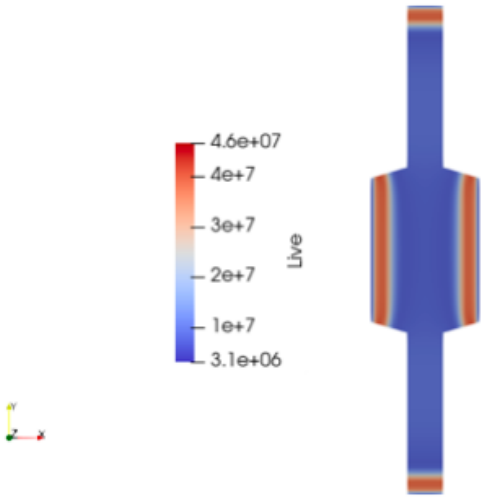

(c) Living cells case with P1 elements

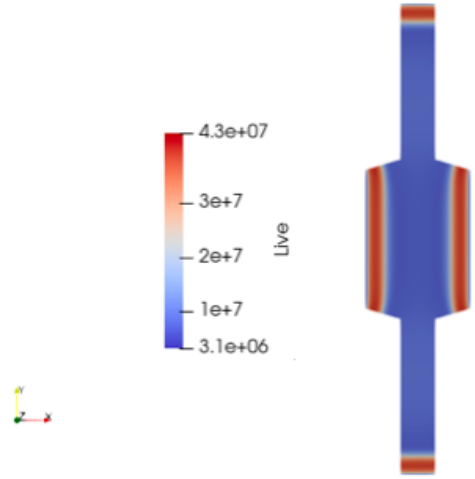

(d) Living cells case with P3 elements

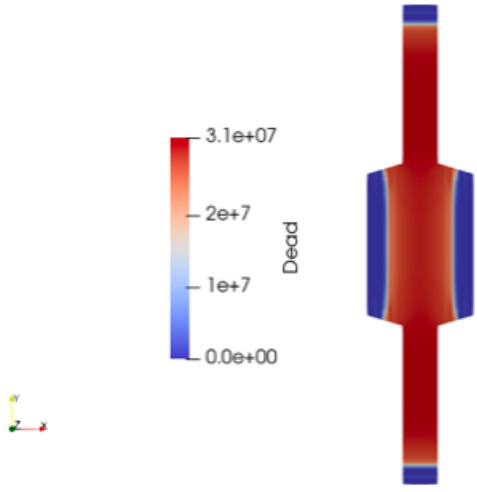

(e) Dead cells case with P1 elements

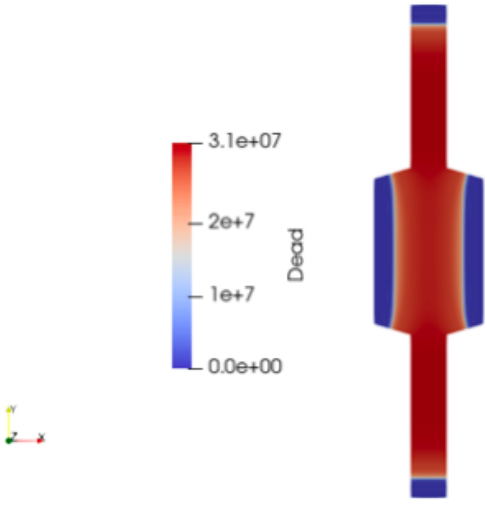

(f) Dead cells case with P3 elements

Figure 6: 2D contour plots for case B of the oxygen, living cells and dead cells after 3 days.

	P1	P3
nOfNodes	1473	12481
nOfElements	1344	1344
theNumOfUnknowns of oxygen and live cells	2862	24718
theNumOfUnknowns of dead cells	1473	12481
time building the linear system of oxygen and live cells	0.87	4.91
time solving the linear system of oxygen and live cells	0.01	7.01
time building the linear system of dead cells	0.33	1.07
time solving the linear system of dead cells	0.01	0.71
approximated cpu time	256.99	2018.45

Table 4: Case B, the number of nodes and elements in each problem and the computational time used to create and solve the system are detailed.

5.1.3 Case C

In this last trial the boundary conditions are a bit different to the previous cases. In concrete, the boundary conditions are:

1. For oxygen:

$$\begin{aligned} \mathbf{f^0}\cdot\mathbf{n} &= 0 \quad \text{in the solid wall.} \\ c^0 &= g^0 \quad \text{in the exchange surface.} \\ c^0 &= g^0 \quad \text{in the valves.} \end{aligned}$$

   with $g^0 = 7\text{mmHg}$.

2. For living cells:

$$\begin{aligned} \mathbf{f^1}\cdot\mathbf{n} &= 0 \quad \text{in the solid wall.} \\ \mathbf{f^1}\cdot\mathbf{n} &= \beta^1 c^1 \quad \text{in the exchange surface.} \\ \mathbf{f^1}\cdot\mathbf{n} &= 0 \quad \text{in the valves.} \end{aligned}$$

   with $\beta^1 = 10^{-6}$ s/cm

3. For dead cells:

$$\begin{aligned} \mathbf{f^2}\cdot\mathbf{n} &= 0 \quad \text{in the solid wall.} \\ \mathbf{f^2}\cdot\mathbf{n} &= 0 \quad \text{in the exchange surface.} \\ \mathbf{f^2}\cdot\mathbf{n} &= 0 \quad \text{in the valves.} \end{aligned}$$

   Note that no flux boundary condition is applied on the exchange wall because in the experiments no dead cells have been observed leaving the micro-chamber (see reference [2] for details).

The results are presented in figure 7. In the first column, we have used a Backward Euler for the temporal discretization with linear elements while the second one corresponds to DIRK3S3 temporal discretization

with elements of degree 3. Red colour expresses the high amount of concentration while blue colour means the opposite, that is, there is a lack of this type of concentration in that part.

This can be appreciated in figure 7. As at the top and bottom borders are imposed Dirichlet boundary conditions for oxygen, the concentration of living cells increases near these contours, while the concentration of dead cells decreases in the vicinity of these contours. Furthermore, considering that the flux of living cells is null, they tend to accumulate in this contour due to the presence of oxygen.

Similar results are obtained in both simulations. Table 5 summarizes the characteristics of the used mesh and the computational time of building and solving the linear systems at each stage of the DIRK scheme.

	P1	**P3**
nOfNodes	1473	12481
nOfElements	1344	1344
theNumOfUnknowns of oxygen and live cells	2862	24718
theNumOfUnknowns of dead cells	1473	12481
time building the linear system of oxygen and live cells	0.93	4.33
time solving the linear system of oxygen and live cells	0.01	8.43
time building the linear system of dead cells	0.34	1.01
time solving the linear system of dead cells	0.01	0.88
approximated cpu time	261.75	2003.33

Table 5: Case C, the number of nodes and elements in each problem and the time required to create and solve the system are detailed.

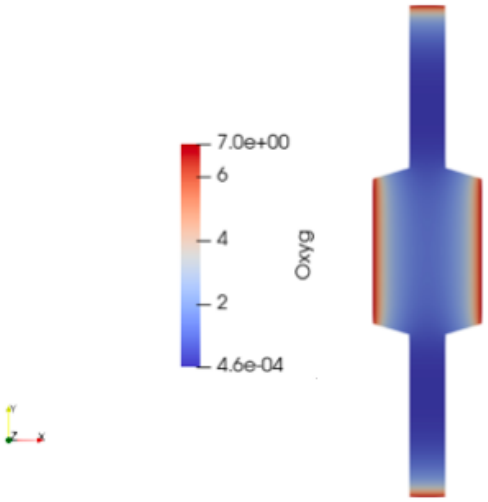

(a) Oxygen case with P1 elements

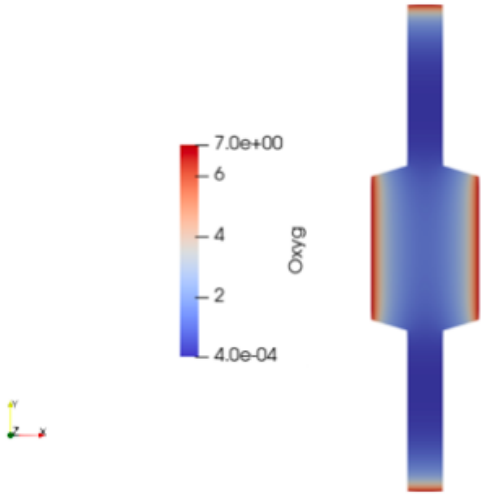

(b) Oxygen case with P3 elements

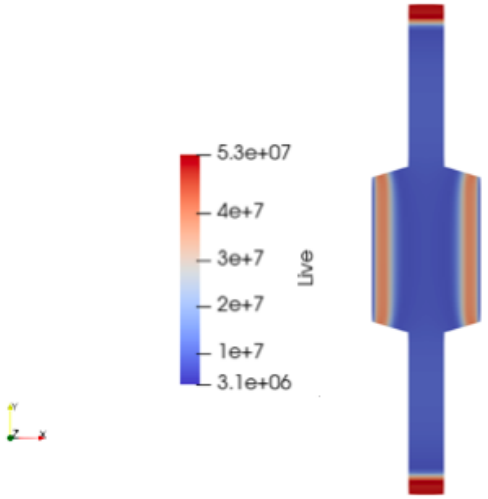

(c) Living cells case with P1 elements

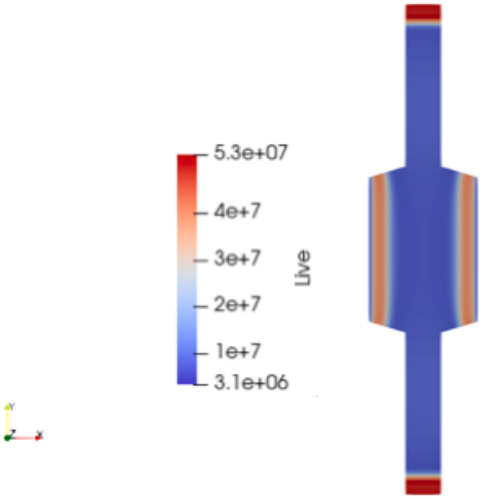

(d) Living cells case with P3 elements

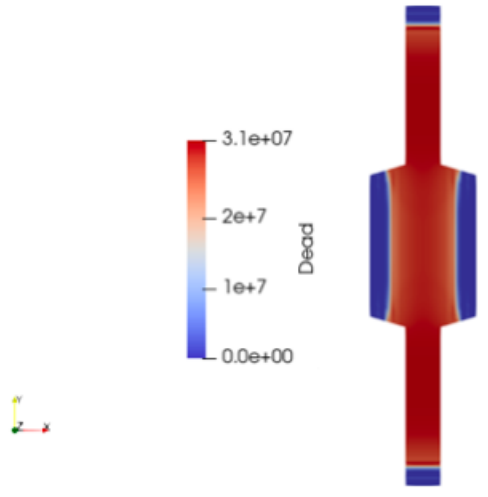

(e) Dead cells case with P1 elements

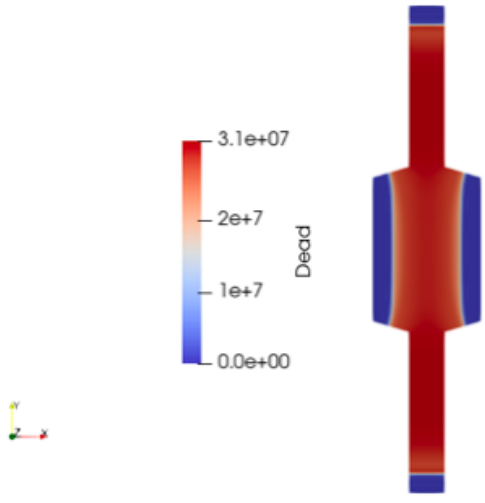

(f) Dead cells case with P3 elements

Figure 7: 2D contour plots for case C of the oxygen, living cells and dead cells after 3 days.

5.2 3D simulation of two microfluidic devices under the same working conditions

In this section we will simulate two microfluidic devices under similar working conditions. On the one hand, the same shape as in 2D models will be used, see figure 8. On the other hand, another chip model will be used, see figure 10.

In both of them a single pallisade will be generated since oxygen will be supplied from one single microchannel when a lower concentration of living cells is inserted in the micro-chamber.Therefore, cells migrate towards the open microchannel more slowly than in the necrotic core case and a pallisade of living cells is generated for the open side.

The initial conditions are:

$$\begin{aligned} c^{0,0} &= 2 \text{ mmHg} \\ c^{1,0} &= 3.99 \times 10^6 \text{ cells/mL} \\ c^{2,0} &= 0 \text{ cell/mL} \end{aligned}$$

With regard to boundary conditions, the oxygen will only be supplied on one of the exchange surface side. Then,

1. For oxygen:

$$\begin{aligned} \mathbf{f^0} \cdot \mathbf{n} &= 0 \quad \text{in the solid wall and one of the exchange surface.} \\ c^0 &= g^0 \quad \text{in the exchange surface.} \\ \mathbf{f^0} \cdot \mathbf{n} &= 0 \quad \text{in the valves.} \end{aligned}$$

   with $g^0 = 2$mmHg

2. For living cells:

$$\begin{aligned} \mathbf{f^1} \cdot \mathbf{n} &= 0 \quad \text{in the solid wall and one of the exchange surface.} \\ \mathbf{f^1} \cdot \mathbf{n} &= \beta^1 c^1 \quad \text{in the other exchange surface.} \\ \mathbf{f^1} \cdot \mathbf{n} &= 0 \quad \text{in the valves.} \end{aligned}$$

   with $\beta^1 = 10^{-9}$ s/cm.

3. For dead cells:

$$\begin{aligned} \mathbf{f^2} \cdot \mathbf{n} &= 0 \quad \text{in the solid wall.} \\ \mathbf{f^2} \cdot \mathbf{n} &= 0 \quad \text{in the exchange surface.} \\ \mathbf{f^2} \cdot \mathbf{n} &= 0 \quad \text{in the valves.} \end{aligned}$$

   Note that no flux boundary condition is applied on the exchange wall because in the experiments no dead cells have been observed leaving the micro-chamber (see reference [2] for details).

Besides that, all simulations have been performed up to a final time step of 8 days and $\Delta t = 2$h. For both cases we have used Backward Euler time integration schemes with linear elements.

5.2.1 First chip model

Figure 8 shows the 3D model analysed in this example. The dimension of this device is 1.35cm high, 0.3 cm wide and 0.02 cm deep. It corresponds to the 3D version of the model simulated in Section 5.1. It can be observed that boundaries coloured in blue represents polymer walls, the green boundary is an exchange surface through which oxygen is supplied and the brown boundary represents the inlet valves.

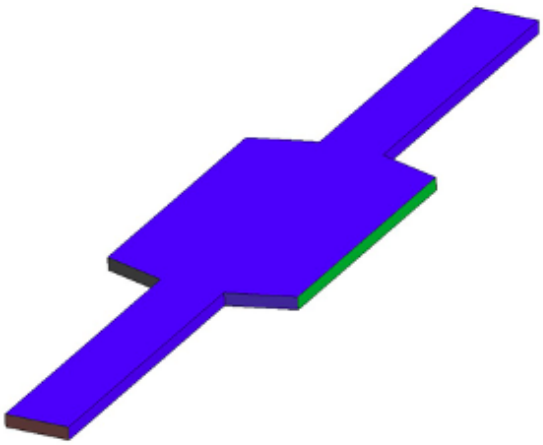

Figure 8: The regions of different boundary conditions in 3D with the first chip model

We consider the same situation as case A of 2D. That is, the valves are closed, acting as a solid wall.

- Oxygen: Neumann homogeneous conditions.
- Living cells: Neumann homogeneous conditions.
- Dead cells: Neumann homogeneous conditions.

Figure 9 shows the concentration distributions after 8 days. Several aspects of these results should be mentioned. First, the oxygen concentration in the inner part of the micro-chamber after 8 days is reduced in a slower rate than the oxygen concentration in the necrotic case. This is due to the fact that the initial concentration of living cells is smaller. Second, the migration of living cells is also smaller due to the fact that there is still oxygen in the inner part of the micro-chamber. Third, since the robin parameter is smaller in the current experiment ($\beta^1 = 10^{-9}$), a smaller living cells concentration does not decay near the exchange surface.

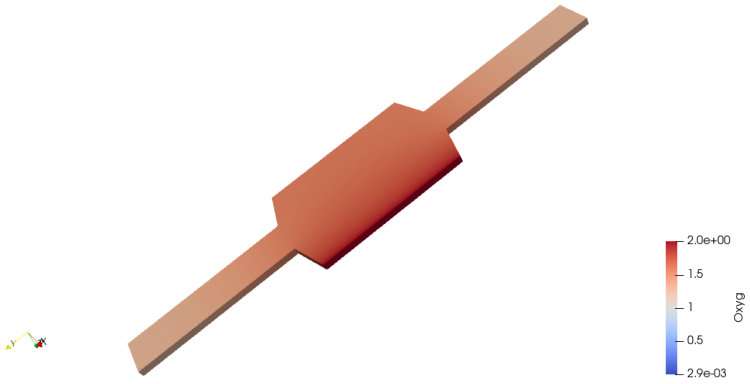

(a) Oxygen case with P1 elements

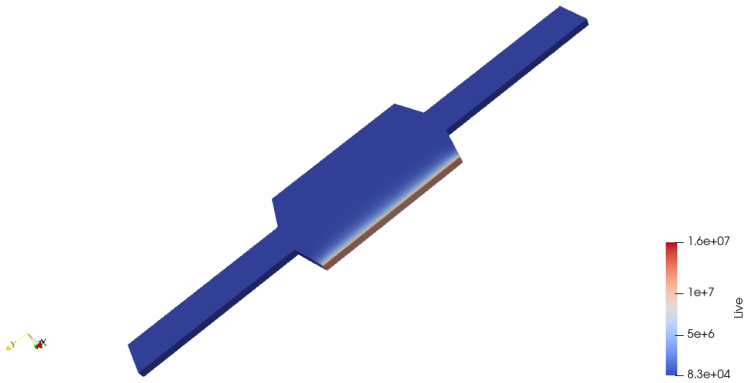

(b) Living cells case with P1 elements

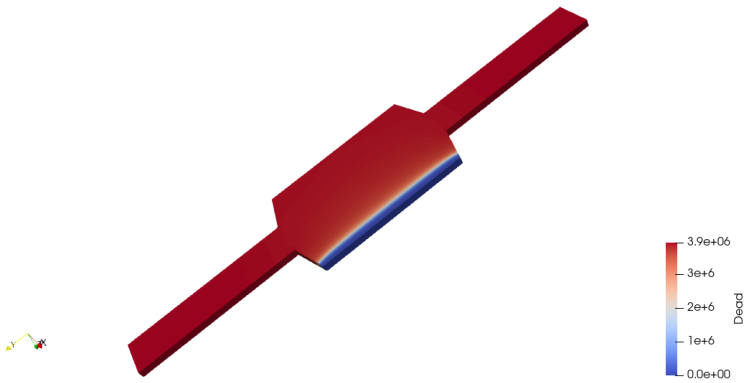

(c) Dead cells case with P1 elements

Figure 9: 3D contour plots of the oxygen, living cells and dead cells in a pseudo pallisade after 8 days.

In table 6, some characteristics of the mesh and the computational time of building and solving the linear system at each stage of the DIRK scheme are summarised. With regard to the computational time, it requires just 6h while *in vitro* experiments need about 8 days to reach a single pallisade state.

	P1
nOfNodes	44415
nOfElements	34240
theNumOfUnknowns of oxygen and live cells	88425
theNumOfUnknowns of dead cells	44415
time building the linear system of oxygen and live cells	25.27
time solving the linear system of oxygen and live cells	18.11
time building the linear system of dead cells	5.65
time solving the linear system of dead cells	2.15
approximated cpu time	22359.27

Table 6: Summarised data of pseudo pallisade with the first chip model.

The number of nodes and elements in each problem and the time required to create and solve the system can be seen.

5.2.2 Second chip model

In this case, the chip model that we have used have a different shape. It is 0.5 cm high, 0.2 cm wide and 0.03 cm deep. Figure 10 shows the CAD model coloured according to the type of boundary. Therefore, according to the type of the prescribed boundary condition.

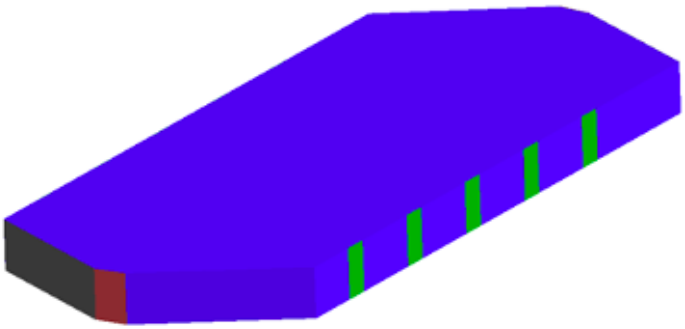

Figure 10: The regions of different boundary conditions in 3D with the second chip model

The blue parts correspond to the polymer walls. Green boundaries represent an exchange surface through which oxygen is supplied. Finally, the brown boundary corresponds to the inlet valves.

Considering the initial and boundary conditions described above, the single pallisade phenomenon can be appreciated in the figure 11.

Observing the three images, we can see that in the valves there is not any exchange of oxygen or cells as we have imposed Neumann homogeneous conditions. With regard to the exchange surface, in the holes, the presence of oxygen and living cells can be appreciated. As expected a pseudo pallisade of living cells is generated next to the exchange surfaces. Moreover, as we move away from the holes, the presence of dead cells is greater.

In table 7, some characteristics about the mesh and the time required to create and solve the system at each stage of the DIRK scheme are summarised.

	P1
nOfNodes	26649
nOfElements	22080
theNumOfUnknowns of oxygen and live cells	53158
theNumOfUnknowns of dead cells	26649
time building the linear system of oxygen and live cells	17.16
time solving the linear system of oxygen and live cells	37.92
time building the linear system of dead cells	3.91
time solving the linear system of dead cells	3.25
approximated cpu time	26548.87

Table 7: Summarised data of pseudo pallisade with the second chip model.

Finally, it can be stated that the require computational time is 7 hours while in a trial 8 days have to be passed.

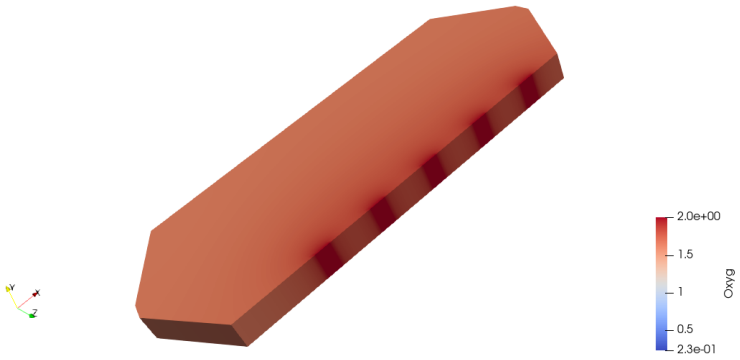

(a) Oxygen case with P1 elements

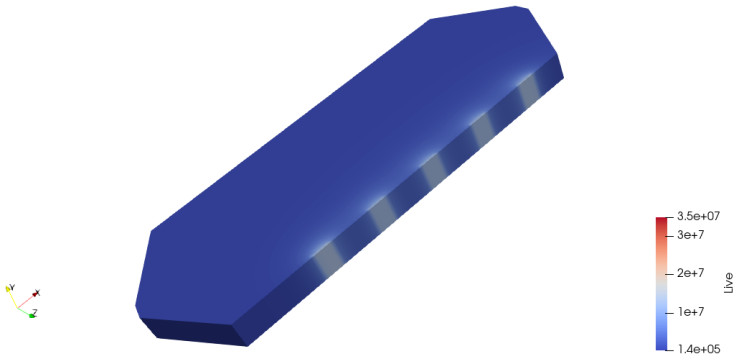

(b) Living cells case with P1 elements

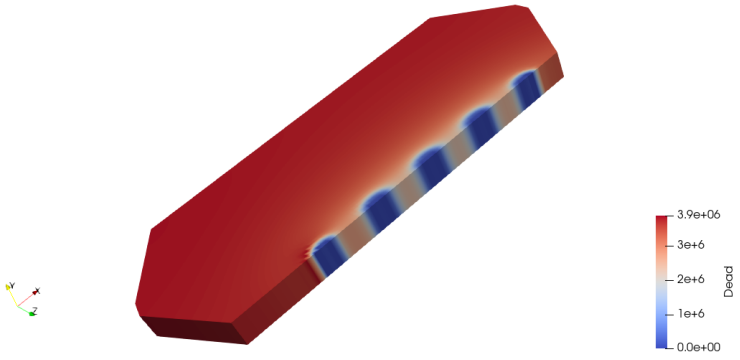

(c) Dead cells case with P1 elements

Figure 11: 3D contour plots of the oxygen, living cells and dead cells of a pseudo pallisade after 8 days.

6. Conclusions and further investigation

In this work we have presented a mathematical model to simulate the growth of glioblastoma in a microfluidic device. It is composed of a system of two non-linear PDE coupled with a non linear ODE. To solve this problem, we use continuous high order finite elements and implicit DIRK time discretization schemes.

In order to improve the computational efficiency of the developed formulation we have exploited the structure of the Jacobian matrix and we have split the global Jacobian in two parts. The first containing the unknowns corresponding to the nodal values of the oxygen and living cells concentration and the other corresponding to the nodal values of dead cells.

We have applied the formulation to several CAD models. In the first one, we have simulated a necrotic core state in 2D model using different space and time discretization methods. In the second one, we have analysed a single pallisade state in 3D version by using two different microfluidic devices.

Several works will be analysed in the near future. First, non-isotropic representation of the diffusive matrices and chemotaxis matrices will be implemented. This is important because non-isotropic hydrogel will be used. Second, iterative solvers will be implemented in order to further improve the computational efficiency of the implementation (reducing the memory footprint and the execution time). This will be of the major importance when dealing with more complex 3D models.

Other aspects can also be explored in the future. From the modelling point of view, gravity effects should be included in order to reproduce the experimental results observed in specific microfluidic devices. From the numerical point of view, other formulation such as hybridizable Discontinuous Galerkin (HDG) should be considered if the convection (due to the migration) of living cells produced by chemotaxis is more relevant.

References

[1] J. Ayensa-Jimeńez, M. Pérez-Aliacar, T. Randelovic, J. A. Sanz-Herrera, M. H. Doweidar, and M. Doblare. Analysis of the parametric correlation in mathematical modeling of in vitro glioblastoma evolution using copulas. *Mathematics*, 9(1):27, 2020.

[2] J. Ayensa-Jimeńez, M. Pérez-Aliacar, T. Randelovic, J. A. Sanz-Herrera, M. H. Doweidar, and M. Doblare. Mathematical formulation and parametric analysis of in vitro cell models in microfluidic devices: application to different stages of glioblastoma evolution. *Scientific Reports*, 10(1):1–21, 2020.

[3] J.C. Butcher. *Numerical methods for ordinary differential equations*. John Wiley & Sons, 2016.

[4] Kenned, A. Christopher, Carpenter, and H. Mark. Diagonally implicit runge-kutta methods for ordinary differential equations. a review. Technical report, 2016.

[5] H. Kitano. Computational systems biology. *Nature*, 420(6912):206–210, 2002.

[6] A. Kriete and R. Eils. *Computational systems biology: From molecular mechanisms to disease*. Academic press, 2013.

[7] S. J. Mousavi, M. Doblaré, and M. H. Doweidar. Computational modelling of multi-cell migration in a multi-signalling substrate. *Physical biology*, 11(2):026002, 2014.

[8] S. J. Mousavi, M. H. Doweidar, and M. Doblaré. 3d computational modelling of cell migration: a mechano-chemo-thermo-electrotaxis approach. *Journal of theoretical biology*, 329:64–73, 2013.

[9] C. Wang, Z. Tang, Y. Zhao, R. Yao, L. Li, and W. Sun. Three-dimensional in vitro cancer models: a short review. *Biofabrication*, 6(2):022001, 2014.